Journal of
Mechanics of
Materials and Structures

SIMULATIONS OF MICRO AND NANOINDENTATIONS

Zishun Liu, Somsak Swaddiwudhipong and Qingxiang Pei

Volume 3, Nº 10 December 2008

mathematical sciences publishers

JOURNAL OF MECHANICS OF MATERIALS AND STRUCTURES
Vol. 3, No. 10, 2008

SIMULATIONS OF MICRO AND NANOINDENTATIONS

ZISHUN LIU, SOMSAK SWADDIWUDHIPONG AND QINGXIANG PEI

The paper reviews recent research and developments on simulated indentation tests at micron and nanometer levels. For indentation at the maximum depth of several microns or hundreds of nanometer, classical continuum plasticity framework incorporating Taylor dislocation model via strain gradient plasticity embedded in the constitutive equation may be adopted to take care of the size effect. As higher-order stress components and higher-order continuity requirements can be made redundant, only C^0 finite elements incorporating strain gradient plasticity have to be formulated. This results in the significant ease and convenience in finite element implementation requiring minimal additional computational effort and resources. Alternatively, when the indentation depth is lower at nanometer level, either a large scale molecular dynamics model or a hybrid finite element and molecular dynamics simulation has to be adopted. The article includes certain results from the former approach on nanoindentation based on combination of both Morse potential and embedded-atom model potential.

1. Introduction

Numerous experiments including indentation tests [Stelmashenko et al. 1993], twisting of copper wires of micron diameters [Fleck and Hutchinson 1993], fracture toughness tests [Elssner et al. 1994] and microbend tests [Haque and Saif 2003] have demonstrated a strong size effect when the material and deformation length scales are of the same order at micron and submicron levels. Classical continuum mechanics ceases to be valid at this range of deformation. Based on the Taylor [1934] dislocation model (see also [Toupin 1962]), Fleck et al. [1994] proposed the phenomenological theory of strain gradient plasticity. Gao et al. [1999] and Huang et al. [2000] presented a multiscale framework for constructing the mesoscale constitutive laws taking into account the microscale plasticity based on Taylor's work hardening relation. Higher-order stress components, additional governing equations and boundary conditions are required in the formulation, requiring significantly greater formulation and computational efforts. Huang et al. [2004] proposed the conventional mechanism-based strain gradient (CMSG) plasticity theory without involving the higher-order stress components. The approach is appealing as only C^0 continuity is required in the finite element formulation. The concept was adopted by Swaddiwudhipong et al. [2005; 2006a; 2006b] to establish solid, axisymmetric and plane finite elements to simulate Berkovich and conical indentation tests at micron and submicron levels and fracture behavior of elastoplastic materials with strain hardening. In this study, both C^0 solid and axisymmetric finite elements are adopted to demonstrate the necessity of incorporating strain gradient plasticity in the simulation of Berkovich and conical indentation tests at submicron level respectively. The effect of friction at contact surfaces is

Keywords: C^0 finite element, indentation test, molecular dynamics simulation, size effect, strain gradient plasticity.
The supports from the Singapore Ministry of Education's AcRF Tier 1 Funds through grants R-214-000-165-112 and R-214-000-186-112 are greatly appreciated.

also considered in the present numerical model. The results obtained from finite element analyses with and without the strain gradient plasticity including both friction and smooth surfaces are presented and compared.

Molecular dynamics (MD) model is effective in the simulation of behavior of nanostrucures, offering the insights into the microscopic properties of materials. MD simulation has recently been used to investigate various aspects of nanomechanics of materials including wear, fracture and characterization of materials at nanometer level. It has been shown that MD simulations can provide a qualitative analysis of discrete plasticity events that are consistent with experimental observations of nanoindentation in single crystals. The approach has become a favorite tool for investigating the physical properties of nano materials at an atomic level [Fang et al. 2001; 2006]. In this study, nanoindentation experiments are simulated using MD simulation adopting embedded-atom model (EAM) potential for target materials and Morse potential for both diamond indenter and interaction between target and indenter materials. The paper covers the mechanisms of nanoindentation on single crystalline substrate using MD simulation. The large scale model is developed for substrate materials in the present MD simulation. Compared with results reported earlier in the literature, the values presented in this article should be less affected by boundary influence.

2. Strain gradient plasticity

The flow stress with Taylor hardening model and the material length scale l for typical values of $M = 3.06$ and $\bar{r} = 1.90$ can be expressed as

$$\sigma_t = \sigma_y \sqrt{f^2(\varepsilon^p) + l\eta^p}, \qquad l = \bar{r}b\Big(\frac{M\alpha\mu}{\sigma_y}\Big)^2 = 18b\Big(\frac{\alpha\mu}{\sigma_y}\Big)^2,$$

where σ_y is the yield stress, $f(\varepsilon^p)$ represents the stress and plastic strain relation in uniaxial tension, η^p implies the effective plastic strain gradient, $\bar{r}$ is the Nye [1953] factor, M is the Taylor factor, b indicates the magnitude of Burgers vector, μ represents the shear modulus and α is an empirical constant, the value of which varies from 0.2–0.5 depending on the material structures. Based on models of geometrically necessary dislocations associated with the in-plane bending, the torsion of a rod and the spherical or axisymmetric void growth, Gao et al. [1999] expressed the effective plastic strain gradient as

$$\eta^p = \tfrac{1}{2}\sqrt{\eta^p_{ijk}\eta^p_{ijk}},$$

where $\eta^p_{ijk} = \varepsilon^p_{ik,j} + \varepsilon^p_{jk,i} - \varepsilon^p_{ij,k}$, with the comma (,) in subscripts indicating the differentiation with respect to the index which follows. ε^p_{ij} is the plastic strain tensor $\varepsilon^p_{ij} = \int \dot{\varepsilon}^p_{ij}\, dt$, where the dot in superscripts implies time derivative. Huang et al. [2004] showed that the constitutive relation for materials with strain gradient plasticity can be expressed as

$$\dot{\sigma}_{ij} = K\dot{\varepsilon}_{kk}\delta_{ij} + 2\mu\left(\dot{\varepsilon}'_{ij} - \frac{3\dot{\varepsilon}}{2\sigma_e}\Big(\frac{\sigma_e}{\sigma_f}\Big)^m \sigma'_{ij}\right), \tag{2-1}$$

where σ_e is the von Mises effective stress and m is the rate-sensitive exponent. Equation (2-1) degenerates to the constitutive relation for materials with power law hardening when m is large, say $m \geq 20$ as shown earlier in [Huang et al. 2004]. It is interesting to note that higher-order stress components are not

explicitly present in the constitutive relation (2-1) though strain gradient plasticity has been incorporated. This approach facilitates the adoption of conventional continuum mechanic algorithms which are readily available to be employed with minor alterations. Hence, the order of continuity requirement for the finite element model can be reduced from C^1 to C^0 level. This provides a substantial simplification in the formulation and implementation of this powerful numerical tool, resulting in minimal additional computational resources and effort. Though higher-order stress theory is normally required in mechanism-based strain gradient (MSG) plasticity, it was shown in [Shi et al. 2001; Huang et al. 2004] that the results based on CMSG plasticity are practically identical to those on MSG in most part of the domain except in the thin layers near the boundary. As the CMSG framework is much less demanding than the higher-order stress theory, the former serves as an efficient alternative approach producing results without any significant loss of accuracy.

3. Effective strain gradient

The strain gradient tensor of third-order η and the displacement vector u are expressed as

$$\eta = \nabla\nabla u\,, \quad u = \sum_i u_i \tilde{e}_i,$$

where $\tilde{e}_i$ is the unit vector in the i-th direction. The expressions for effective strain gradient plasticity in Cartesian coordinate system are standard and hence not given herein. The components for axisymmetric case were derived in [Swaddiwudhipong et al. 2006b]:

$$\eta'_{rrr} = \tfrac{1}{2}\eta_{rrr} - \tfrac{1}{2}(\eta_{rtt} + \eta_{rzz}) = \tfrac{1}{2}u_{rcrr} - \tfrac{1}{2}\left(\left(\frac{u_{rcr}}{r} - \frac{u_{rr}}{r^2}\right) + u_{zczr}\right),$$

$$\eta'_{rrz} = \eta_{rrz} = u_{zcrr}\,, \qquad \eta'_{zzr} = \eta_{zzr} = u_{rczz}\,,$$

$$\eta'_{rtt} = \eta'_{trt} = \tfrac{3}{4}\eta_{rtt} - \tfrac{1}{4}(\eta_{rrr} + \eta_{rzz}) = \tfrac{3}{4}\left(\frac{u_{rcr}}{r} - \frac{u_{rr}}{r^2}\right) - \tfrac{1}{4}(u_{rcrr} + u_{zczr})\,,$$

$$\eta'_{rzr} = \eta'_{zrr} = \tfrac{3}{4}\eta_{rzr} - \tfrac{1}{4}\eta_{ztt} + \eta_{zzz}) = \tfrac{3}{4}u_{rczr} - \tfrac{1}{4}\left(\frac{u_{rcz}}{r} + u_{zczz}\right),$$

$$\eta'_{rzz} = \eta'_{zrz} = \tfrac{3}{4}\eta_{rzz} - \tfrac{1}{4}(\eta_{rrr} + \eta_{rtt}) = \tfrac{3}{4}u_{zczr} - \tfrac{1}{4}\left(u_{rcrr} + \left(\frac{u_{rcr}}{r} - \frac{u_{rr}}{r^2}\right)\right),$$

$$\eta'_{ttr} = \eta_{ttr} = \frac{u_{rcr}}{r} - \frac{u_{rr}}{r^2}\,, \qquad \eta'_{ttz} = \eta_{ttz} = \frac{u_{zcr}}{r}\,,$$

$$\eta'_{tzt} = \eta'_{ztt} = \tfrac{3}{4}\eta_{tzt} - \tfrac{1}{4}(\eta_{zrr} + \eta_{zzz}) = \tfrac{3}{4}\frac{u_{rcz}}{r} - \tfrac{1}{4}(u_{rcrz} + u_{zczz})\,,$$

$$\eta'_{zzz} = \tfrac{1}{2}\eta_{zzz} - \tfrac{1}{2}(\eta_{zrr} + \eta_{ztt}) = \tfrac{1}{2}u_{zczz} - \tfrac{1}{2}\left(u_{rcrz} + \frac{u_{rcz}}{r}\right),$$

where subscript r, θ and z denote orthogonal cylindrical coordinates.

4. C^0 elements with strain gradient plasticity

The coordinates of C^0 solid elements are usually expressed as

$$x = \sum_{i=1}^{n} N_i(g,h,r)\, x_i\,, \qquad y = \sum_{i=1}^{n} N_i(g,h,r)\, y_i\,, \qquad z = \sum_{i=1}^{n} N_i(g,h,r)\, z_i\,,$$

and the displacements of C^0 solid elements are usually expressed as

$$u = \sum_{i=1}^{n} N_i(g,h,r)\, u_i\,, \qquad v = \sum_{i=1}^{n} N_i(g,h,r)\, v_i\,, \qquad w = \sum_{i=1}^{n} N_i(g,h,r)\, w_i\,,$$

and the Jacobian matrix which is essential for the transformation of coordinates is obtained from

$$J = \frac{\partial(x,y,z)}{\partial(g,h,r)} = \begin{pmatrix} x_{,g} & x_{,h} & x_{,r} \\ y_{,g} & y_{,h} & y_{,r} \\ z_{,g} & z_{,h} & z_{,r} \end{pmatrix}.$$

In each element, n is the number of nodes; x_i, y_i, z_i and u_i, v_i, w_i are the nodal coordinates and nodal displacement components in the x, y and z directions respectively while g, h and r are the corresponding natural coordinates.

The derivative of the strain vector with respect to x is given by

$$\{\varepsilon\}_{,x} = \left(\frac{\partial^2 u}{\partial x^2}\,,\ \frac{\partial^2 v}{\partial y \partial x}\,,\ \frac{\partial^2 w}{\partial y \partial x}\,,\ \frac{\partial^2 u}{\partial y \partial x} + \frac{\partial^2 v}{\partial x^2}\,,\ \frac{\partial^2 v}{\partial z \partial x} + \frac{\partial^2 w}{\partial y \partial x}\,,\ \frac{\partial^2 w}{\partial x^2} + \frac{\partial^2 u}{\partial z \partial x} \right)^T = [B]_{,x}\{\delta\}\,,$$

while the coordinate transformation of the derivatives of finite element displacement functions of the actual and master elements is stipulated by

$$\frac{\partial(N_{i,x}, N_{i,y}, N_{i,z})}{\partial(x,y,z)} = (J^{-1})^T \frac{\partial(N_{i,g}, N_{i,h}, N_{i,r})}{\partial(g,h,r)} J^{-1}\,.$$

Details of the derivation were presented earlier in [Swaddiwudhipong et al. 2005]. Similar derivations of strain gradient measures and coordinate transformation for axisymmetric and plane elements are presented in [Swaddiwudhipong et al. 2006b; 2006a], respectively. The concept is implemented as a user subroutine in a commercial finite element package, ABAQUS [ABAQUS 2002].

5. Molecular dynamics simulation

In this study, the standard MD technology as described in details in [Rapaport 2004] is used to simulate the motion of the atoms of the materials. Equations of motions are integrated using Verlet method. In MD simulations, the force acting on an individual atom is obtained by summing up the forces contributed by the surrounding atoms. The interatomic forces are calculated from the potential energy function U :

$$\mathbf{f}_i = -\nabla U(\mathbf{r}_1, \mathbf{r}_2, \ldots, \mathbf{r}_N)\,.$$

The main problem for modeling the material in MD simulations is to find a suitable potential function $U(\mathbf{r}_1, \mathbf{r}_2, \ldots, \mathbf{r}_N)$. The pair potential is relatively simple and computational inexpensive, but it is less accurate compared to the embedded-atom model (EAM) potential. The EAM potential is based upon the recognition that the cohesive energy of a metal is governed not only by the pairwise potential of the nearest neighbor atoms, but also by the embedding energy related to the electron sea in which the atoms are embedded. The total energy E_{tot} which can be written as a unique function of the electron density r_{ij} is mainly the energy to embed the atoms into the electron sea of the neighboring atoms,

and supplemented by a short-range doubly screened pair interaction, which accounts for the core-core repulsions. Consequently, the total atomic potential energy of a system [Pei et al. 2006] is given by

$$E_{tot} = \tfrac{1}{2}\sum_{i,j} \Phi_{ij}(r_{ij}) + \sum_i F_i(\bar{\rho}_i),$$

where Φ_{ij} is the pair-interaction energy between the i-th and the j-th atoms, F_i represents the embedding energy of atom i, and $\bar{\rho}_i$ indicates the host electron density at site i induced by all other atoms in the system. In this paper, the EAM potential is used for the atomic interaction among the nickel (Ni) atoms of the target substrate materials. The Morse potential is, however, adopted for the interaction between the atoms of nickel substrate and those of diamond indenter. The Morse type pair potential is given by

$$\phi(r_{ij}) = D\left(e^{-2\beta(r_{ij}-r_0)} - 2e^{-\beta(r_{ij}-r_0)}\right),$$

where $\phi(r_{ij})$ is the pair potential energy function, D is the cohesion energy, β represents the elastic modulus, and r_{ij} and r_0 are the instantaneous and equilibrium distances between atoms i and j, respectively. The Morse potential is also employed for the interaction among the atoms of the diamond indenter. The latter is usually assumed as a rigid body since the diamond is substantially harder than the nickel substrate. This implies that the interactive forces among the indenter atoms have no bearing on the accuracy of the simulated force results.

6. Numerical examples

6A. ***Simulation of indentation at micron level via finite elements with strain gradient plasticity.*** Both conventional finite elements and those incorporating mechanism-based strain gradient plasticity are employed by Pethica et al. [1983] to simulate the Berkovich indentation on electropolished nickel. The following material properties adopted earlier in [Bhattacharya and Nix 1988] to simulate this test are employed in the study. The Young's modulus of elasticity $E = 207\,\text{GPa}$, the yield strength $Y = 350\,\text{MPa}$, $n = 0.03$ in the power law, and the Poisson's ratio $v = 0.33$. The friction coefficient of 0.15 which is typical for contact surfaces of metallic materials and diamond indenter is adopted in the analyses. The intrinsic material length scale of 5 micron for nickel as stipulated in [Wang et al. 2003] is used in the analyses. These finite element analyses include both friction and smooth contact surfaces. The typical computing time required for each simulation carried out in this study using Sun Blade 2000 Workstation 2@900 MHz with 1 GB RAM are about 6 and 30 hours for conical and Berkovich indentation tests respectively.

Figure 1 compares the solutions obtained from finite element analyses with and without the strain gradient effects are compared with the experimental data reported in [Pethica et al. 1983]. The comparison demonstrates clearly the hardening effects of materials subject to indentation at micron and submicron levels. Numerical results obtained from the finite element model incorporating CMSG plasticity theory agree rather well with indentation test results. In contrast, conventional finite element solutions deviate significantly from the test results conducted at submicron level. The numerical results obtained from the proposed axisymmetric and solid finite elements are by and large identical.

6B. ***Molecular dynamics simulation for nanoindentation.*** In this study, the simulations of the nanoindentation on a fcc crystalline nickel substrate by a covalently bonded hemisphere diamond tip has been carried out. The positions and velocities of both the tip and the substrate atoms were obtained as functions

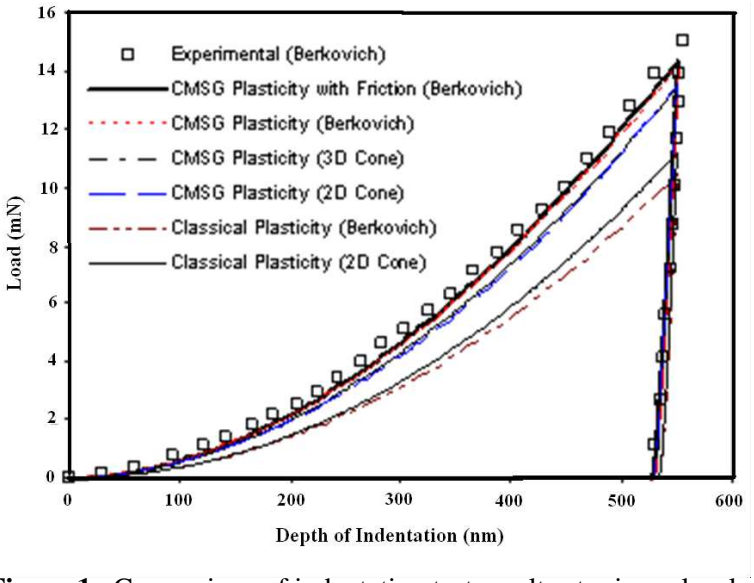

Figure 1. Comparison of indentation test results at micron level.

of time using the MD method. It is assumed that the heat generated in the system during the indentation process was dissipated by the thermal baths of the tip and of the substrate at a high rate that is much faster than the indentation speed. Therefore, in the simulations the nano scale tip and substrate were controlled at the same temperatures during the indentations, that is, the indentations are considered as isothermal processes.

The configuration of the simulated tip and substrate is shown in Figure 2. The substrate material is nickel having fcc lattice with a lattice constant of 3.52 Å. The substrate sizes are 35.2 nm × 35.2 nm × 35.2 nm containing 4,000,000 atoms. A hemisphere (radius = 10.5 nm) diamond indenter is used. The

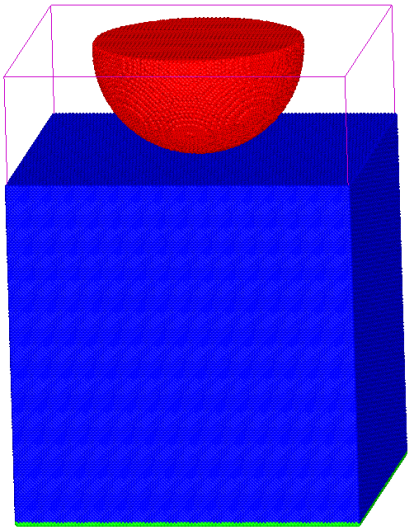

Figure 2. Large scale MD simulation model containing more than 4 million atoms.

latter contains 289,235 carbon atoms. The typical CPU time required for each MD simulation carried out in the present study is about 200 hours based on IBM p575 supercomputer. The boundary conditions of the substrate include:

(1) The two layers of atoms at the bottom of the substrate are fixed in space while the top surface of the substrate is free.

(2) Periodic boundary conditions are applied at the four side surfaces of the substrate. The indentation is on the (001)-surface of the fcc lattice.

The load-displacement curve obtained from the MD simulated indentation test on nickel as depicted in Figure 3 shows as expected that the indentation depth increases with loading. The load-displacement response, which depicts the force required to push the indenter tip a certain distance into the substrate, demonstrates characteristic discontinuities. Examining the load-displacement curve in detail, we find the first significant drop occurs at the indentation depth of about 1 nm. This drop, representing a transition from elastic to plastic deformation, is attributed to the nucleation of a dislocation. It can be further observed that the initial loading region of the load-displacement curve can be assumed to be linear and the reduced Young's modulus of elasticity can be determined through the relationship $F = 2E_r r_a h$, where F is the loading force, E_r is the reduced Young's modulus, r_a is the radius of contact area, and h is the penetration depth. The atomic configuration at about 1.3 nm indentation depth, the associated Von Mises stress contours in the nanoindentation process are illustrated in Figure 4, left, while the dislocations in the substrate materials are shown in Figure 4, right. The results demonstrate that plastic deformation takes place near the contact area and the dislocations of substrate materials occur beneath the contact

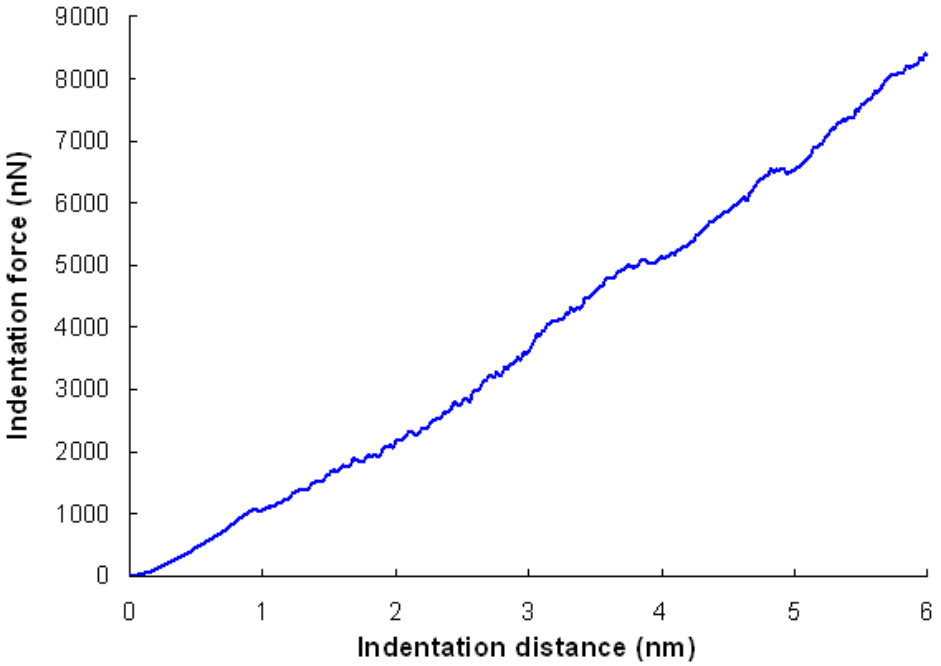

Figure 3. Variation of indentation force against indentation distance.

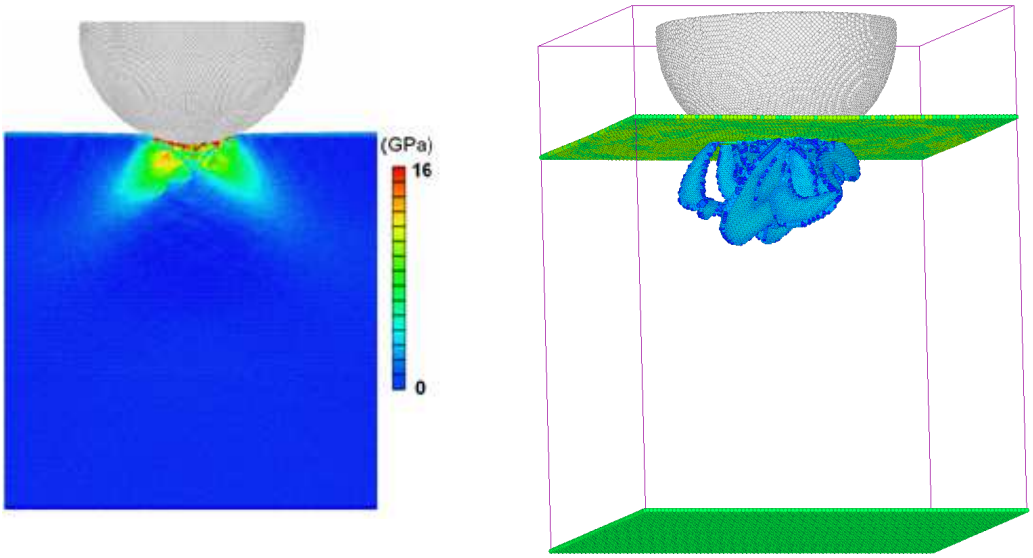

Figure 4. Left: Stress (von Mises) distribution in the substrate during nanoindentation simulation. Right: Dislocations in nickel substrate during indentation.

surface. These phenomena are consistent with the MD simulated results of copper as reported in [Saraev and Miller 2005].

7. Conclusions

A C^0 finite element approach for materials with strain gradient plasticity is proposed in the simulation of indentation tests at the micron and hundreds of nanometers levels. As only the constitutive condition is affected, higher-order stress and hence higher-order continuity requirements are no longer necessary. The elements were adopted to simulate the Berkovich indentation on electropolished nickel. Comparison of finite element results with other existing analytical solutions demonstrates that when the material length scale and the nonuniform plastic deformation are of the same order at micron or submicron level, the effects of strain gradient plasticity have to be considered. A large scale study using molecular dynamics method to simulate nanoindentation of nickel substrate was also carried out. The load-displacement response, stress variation and the plastic dislocations in the nickel substrate are presented. The paper provides appropriate numerical tools for the simulations of indentation tests at both micron and a few nanometer levels.

References

[ABAQUS 2002] *ABAQUS user's manual*, Version 6.3, Hibbitt and Karlsson and Sorensen, Pawtucket, RI, 2002.

[Bhattacharya and Nix 1988] A. K. Bhattacharya and W. D. Nix, "Finite element simulations of indentation experiments", *Int. J. Solids Struct.* **24**:9 (1988), 881–891.

[Elssner et al. 1994] G. Elssner, D. Korn, and M. Rühle, "The influence of interface impurities on fracture energy of UHV diffusion bonded metal-ceramic bicrystals", *Scr. Metall. Mater.* **31**:8 (1994), 1037–1042.

[Fang et al. 2001] T. H. Fang, C. I. Weng, J. G. Chang, and C. C. Hwang, "Nanotribology of amorphous hydrogenated carbon films using scanning probe microscopy", *Thin Solid Films* **396**:1–2 (2001), 167–173.

[Fang et al. 2006] T. H. Fang, W. J. Chang, and C. I. Weng, "Nanoindentation and nanomachining characteristics of gold and platinum thin films", *Mater. Sci. Eng. A* **430**:1–2 (2006), 332–340.

[Fleck and Hutchinson 1993] N. A. Fleck and J. W. Hutchinson, "A phenomenological theory for strain gradient effects in plasticity", *J. Mech. Phys. Solids* **41**:12 (1993), 1825–1857. MR 94g:73020

[Fleck et al. 1994] N. A. Fleck, G. M. Muller, M. F. Ashby, and J. W. Hutchinson, "Strain gradient plasticity: Theory and experiment", *Acta Metall. Mater.* **42**:2 (1994), 475–487.

[Gao et al. 1999] H. Gao, Y. Huang, W. D. Nix, and J. W. Hutchinson, "Mechanism-based strain gradient plasticity, I: Theory", *J. Mech. Phys. Solids* **47**:6 (1999), 1239–1263. MR 2000k:74014

[Haque and Saif 2003] M. A. Haque and M. T. A. Saif, "Strain gradient effect in nanoscale thin films", *Acta Mater.* **51**:11 (2003), 3053–3061.

[Huang et al. 2000] Y. Huang, H. Gao, W. D. Nix, and J. W. Hutchinson, "Mechanism-based strain gradient plasticity, II: Analysis", *J. Mech. Phys. Solids* **48**:1 (2000), 99–128. MR 2000k:74015

[Huang et al. 2004] Y. Huang, S. Qu, K. C. Hwang, M. Li, and H. Gao, "A conventional theory of mechanism-based strain gradient plasticity", *Int. J. Plast.* **20**:4–5 (2004), 753–782.

[Nye 1953] J. Nye, "Some geometrical relations in dislocated crystals", *Acta Metall.* **1**:2 (1953), 153–162.

[Pei et al. 2006] Q. X. Pei, C. Lu, F. Z. Fang, and H. Wu, "Nanometric cutting of copper: A molecular dynamics study", *Comput. Mater. Sci.* **37**:4 (2006), 434–441.

[Pethica et al. 1983] J. B. Pethica, R. Hutchings, and W. C. Oliver, "Hardness measurement at penetration depths as small as 20 nm", *Philos. Mag. A* **48**:4 (1983), 593–606.

[Rapaport 2004] D. C. Rapaport, *The art of molecular dynamics simulation*, 2nd ed., Cambridge University Press, Cambridge, 2004.

[Saraev and Miller 2005] D. Saraev and R. E. Miller, "Atomistic simulation of nanoindentation into copper multilayers", *Model. Simul. Mater. Sci. Eng.* **13**:7 (2005), 1089–1099.

[Shi et al. 2001] M. Shi, Y. Huang, H. Jiang, K. C. Hwang, and M. Li, "The boundary-layer effect on the crack tip field in mechanism-based strain gradient plasticity", *Int. J. Fract.* **112**:1 (2001), 23–41.

[Stelmashenko et al. 1993] N. A. Stelmashenko, A. G. Walls, L. M. Brown, and Y. V. Milman, "Microindentation on W and Mo oriented single crystals: An STM study", *Acta Metall. Mater.* **41**:10 (1993), 2855–2865.

[Swaddiwudhipong et al. 2005] S. Swaddiwudhipong, J. Hua, K. K. Tho, and Z. S. Liu, "C^0 solid elements for materials with strain gradient effects", *Int. J. Numer. Methods Eng.* **64**:10 (2005), 1400–1414.

[Swaddiwudhipong et al. 2006a] S. Swaddiwudhipong, J. Hua, K. K. Tho, and Z. S. Liu, "Finite element modelling for materials with size effect", *Model. Simul. Mater. Sci. Eng.* **14**:7 (2006), 1127–1137.

[Swaddiwudhipong et al. 2006b] S. Swaddiwudhipong, K. K. Tho, J. Hua, and Z. S. Liu, "Mechanism-based strain gradient plasticity in C^0 axisymmetric element", *Int. J. Solids Struct.* **43**:5 (2006), 1117–1130.

[Taylor 1934] G. I. Taylor, "The mechanism of plastic deformation of crystals, I: Theoretical", *Proc. R. Soc. Lond. A* **145**:855 (1934), 362–387.

[Toupin 1962] R. A. Toupin, "Elastic materials with couple-stresses", *Arch. Ration. Mech. An.* **11**:1 (1962), 385–414. MR 26 #2056

[Wang et al. 2003] W. Wang, Y. Huang, K. J. Hsia, K. X. Hu, and A. Chandra, "A study of microbend test by strain gradient plasticity", *Int. J. Plast.* **19**:3 (2003), 365–382.

Received 5 Jul 2007. Revised 15 Nov 2007. Accepted 6 Dec 2007.

ZISHUN LIU: liuzs@ihpc.a-star.edu.sg
Institute of High Performance Computing, 1 Science Park Road, # 01-01, Singapore 117528

SOMSAK SWADDIWUDHIPONG: cvesomsa@nus.edu.sg

Department of Civil Engineering, National University of Singapore, E1A-07-03, 1 Engineering Drive 2, Singapore 119260
http://www.eng.nus.edu.sg/civil/people/cvesomsa/somsa.html

QINGXIANG PEI: peiqx@ihpc.a-star.edu.sg
Institute of High Performance Computing, 1 Science Park Road, # 01-01, Singapore 117528